RSC Advances

ROYAL SOCIETY OF CHEMISTRY

www.rsc.org/advances

Antibacterial and hemostatic performance of chitosan-organic rectorite/alginate composite sponge

Honghui Zhang [a,1], Xiaoxing Lv [a,1], Xinping Zhang [b,1], Hongjun Wang [c], Hongbing Deng [d], Yuejun Li [a], Xiaoli Xu [a], Rong Huang [a,**], Xueyong Li [a,*]

[a] *Department of Plastic Surgery, Tangdu Hospital, Fourth Military Medical University, Xi'an 710038, China*

[b] *Department of General Surgery, the General Hospital of Shenyang Military, Shenyang 110015, China*

[c] *Department of Chemistry, Chemical Biology and Biomedical Engineering, Stevens Institute of Technology, Hoboken, NJ 07030, USA*

[d] *School of Resource and Environmental Science, Wuhan University, Wuhan 430079, China*

* Corresponding author. Department of Plastic Surgery, Tangdu Hospital, Fourth Military Medical University, Xi'an, Shaan Xi, 710038, China.

Tel: +86 29 84777440; Fax: +86 29 84777440

E-mail address: lixueyong641123@163.com

** Corresponding author. Department of Plastic Surgery, Tangdu Hospital, Fourth Military Medical University, Xi'an, Shaan Xi, 710038, China.

Tel: +86 29 84777440; Fax: +86 29 84777440

E-mail address: 19881208huang@163.com

[1] co-first author with the same contribution to this work.

Abstract

This study reported the preparation and properties of chitosan (CS)-organic rectorite (OREC)/sodium alginate (SA) composite sponge. The novel sponge was fabricated by solution intercalation and chemical cross-linking techniques. The structure and composition of CS/SA and CS-OREC/SA composite sponges were characterized by FE-SEM, FT-IR, XRD and EDX. The results showed that the polyelectrolyte with a highly cross-linked structure and uniform pore distribution could be obtained by mixing CS and SA with or without the addition of OREC into them. Besides, the low cytotoxicity and excellent antibacterial efficacy of prepared CS/SA and CS-OREC/SA sponges were demonstrated by MTT assay and antibacterial assay. Moreover, the results of the hemostatic test on ear-artery, ear-vein and liver injury of rabbit showed that the addition of OREC into the CS/SA composite sponge significantly improved the hemostatic efficiency of as-prepared sponge without compromising the biocompatibility and antibacterial property of CS. This study indicated that the CS-OREC/SA composite sponge had the potential to be potent hemostat for controlling wound infection and bleeding in medical fields.

Keywords*:* chitosan; organic rectorite; sodium alginate; antibacterial; hemostatic efficacy

1. Introduction

In recent years, uncontrolled bleeding is recognized as the leading cause of prehospital trauma deaths in combat settings [1, 2] and the second leading cause of death in civilian trauma [3]. Considering the severity of wartime injuries and associated hemorrhagic deaths, early and effective hemorrhage control of hemorrhage by applying hemostatic agents is of considerable significance to save more lives. On this condition, the profound importance of hemorrhage control has prompted a surge of development of novel hemostatic agents toward this goal.

Over the past decades, considerable efforts have been devoted to the development of hemostatic agents that can control hemorrhage and promote patients' own blood clotting to achieve hemostasis. Though some encouraging results are achieved, there are disadvantages of the commercial hemostatic agents that can not be neglected. The most commonly used hemostatic agents include absorbable gelatin sponges (Gelsponge), bovine-derived microfibrillar collagen (Avitene), and oxidized regenerated cellulose (Surgicel) which is often combined with bovine thrombin. The efficacy of these agents may vary significantly and has not been assessed by vigorous clinical trials, some of them are reported to complicate tissue healing by forming a nidus for infection and abscess formation in severe hemorrhage [4]. Besides, the HemCon chitosan (CS) dressing and the QuikClot zeolite are being used routinely in the battlefield [5, 6]. However, the application of QuikClot is strictly limited because it generates heat that can cause burn injuries, and it has been found that neither QuikClot nor HemCon has survival benefit over gauze in more extreme animal

models of hemorrhage [7, 8]. Thus how to design and fabricate an ideal hemostatic dressing that can control bleeding is a very important and challenging issue.

Of note, the growing incidence of infection by antibiotic-resistant bacteria strains in combat trauma wounds is another challenging issue for caregivers. Though broad spectrum antibiotics has been implicated in the selection of resistant pathogens, antibiotic prophylaxis is still the standard of care since it may be difficult to get early surgical debridement to reduce wound bacteria bioburden under combat conditions [9]. To solve this problem, alternatives to antibiotics should be used to manage wound infection. Ionic silver, an active agent against a wide range of pathogens including multi-drug resistant strain [10], is investigated by many researchers as first line intervention to stop the progress of infection that can lead to septicemia and death, Zhong *et al* reported the quaternized carboxymethyl chitosan (QCMC)/sodium alginate (SA) composite sponge with Ag NP-loaded quaternized carboxymethyl chitosan/organic rectorite (QCORAg) nanocomposite which showed excellent antibacterial and hemostatic properties [11]. Besides, Shin-Yeu Ong *et al* prepared silver-loaded CS dressing by incorporating a procoagulant (polyphosphate) with potent hemostatic and antimicrobial properties [12]. However, Poon *et al* examined the effects of silver on keratinocytes and fibroblasts in another *in vitro* study with applying silver nitrate solution. They demonstrated that silver was toxic to skin cells, fibroblasts and keratinocytes as well as to bacteria [13, 14].

In view of the dual challenges of bleeding and contamination in combat wounds, the ideal hemostatic agent should possess the ability to rapidly stop large-vessel

arterial and venous bleeding even when applied through a pool of blood with bactericidal activity associated with durability and stability at various temperatures and humidities. More importantly, it should be harmless to both the wounded individual and the one giving aid [15, 16]. From this point of view, we conceived a CS-based dressing with improved hemostatic and antimicrobial properties. As we know, CS is an attractive biomaterial for wound care because of its biocompatibility, non-toxicity [17], biodegradability [18] and intrinsic hemostatic [19-21] and antimicrobial properties [22, 23]. Besides, SA wound dressings with excellent biocompatibility, promotion of wound healing and hemostatic function, are widely used in biomedical applications [24, 25]. However, CS's antimicrobial action is limited against certain species of bacteria and in non-acidic pH environments [26]. Among all the adjuvant bacteriostatic agent, organic rectorite (OREC), modified from REC, which is a kind of layered silicate, exhibits larger interlayer distance [27], better separable layer thickness and larger aspect ratio than montmorillonite (MMT) [28]. Besides, the European Food Safety Authority (EFSA) reported that bentonite (dioctahedral montmorillonite), another kind of layered silicate, was safe as a food additive [29]. The tunable interlayer distance of OREC could obviously affect the efficiency of its application, such as adsorption ability [30] and bacteria inhibition [31]. In our previous reports, it was interesting to note that with the addition of OREC, the bacterial inhibition ability of other antibacterial agents could be remarkably enhanced [23]. Hence, we hypothesized that the addition of OREC to CS can lead to a more potent hemostat with improved antimicrobial efficiency.

This paper reported the preparation of a novel intercalated CS-OREC/SA composite sponge with excellent hemostatic efficacy via solution intercalation, cross-linking and freeze-drying techniques. The morphology and compositions of the prepared CS/SA and CS-OREC/SA sponges were investigated by FE-SEM, FT-IR, XRD and EDX analysis. Besides, the biocompatibility of the prepared samples was compared by MTT assay. Moreover, the CS-OREC/SA composite sponge was then compared with CS/SA in disk diffusion test against two common wound pathogens, the Gram-negative bacteria E. coli and Gram-positive bacteria S. aureus *in vitro*. Furthermore, the hemostatic efficacy of CS-OREC/SA composite sponge was systematically demonstrated by auricular artery, marginal auricular vein and liver injury models.

2. Experimental

2.1. Materials

2.1. Materials

Chitosan (CS, M_W =2.1×10^5 Da, DD= 92%) was provided by Yuhuan Ocean Biochemical Co. (Taizhou, China). Sodium alginate (SA, Mw = 2.5×10^5 kDa) was supplied by Aladdin Chemical Reagent Co., China. Calcium rectorite (Ca^{2+}-REC) was obtained from Hubei Mingliu Inc. Co. (Wuhan, China). Cetyltrimethyl ammonium bromide (CTAB) was supplied by Xinrui Science and Technology Inc. Co. (Wuhan, China). All other chemicals were of analytical grade and used as received. Purified water was prepared by a system consisting of three units (active charcoal, ion exchanger, and reverse osmosis) connected in series to an ELGA water purification system (PURELAB ultra, UK). All aqueous solutions were prepared with purified water (electrical resistivity =18.2 MΩ·cm).

Organic rectorite (OREC) and intercalated CS-OREC composites with the mass ratio of 100/1 were synthesized according to the previous reports [32, 33]. Briefly, the OREC was prepared by a cation exchange between Ca^{2+}-rectorite galleries and CTAB in an aqueous solution as described previously [34]. CS-OREC solution with the total concentration of 2% were obtained by adding CS solution dropwise and slowly into OREC suspensions at 60ºC under gentle agitation for 12 h [35].

2.2. Preparation of CS-OREC/SA composite sponges

CS and SA were dissolved in 2% acetic acid solution and purified water to get 2% CS solution and 2% SA solution (w/v), respectively. The above two solutions were

fully mixed and stirred in a volume ratio of 3:1 (SA: CS), then the composites with CS-OREC mentioned above and SA were obtained after the same treatment and homogenized to obtain the CS-OREC/SA . After being deaerated under vacuum to remove entrapped airbubbles, the blends were injected into a home-made mould (10 cm×10 cm×2 cm) and lyophilized at -40ºC. Then the dried samples were soaked in $CaCl_2$ solution for 2h, which was followed by washing with distilled water and lyophilizing again. The composite sponges were obtained and designated as CS/SA and CS-OREC/SA.

2.3. Characterization

The microstructure and composition of as-prepared samples were analyzed using field emission scanning electron microscopy (FE-SEM) and energy-dispersive X-ray (EDX) spectroscopy (FE-SEM, JSM-6700F, JEOL, Japan). The surface and cross-section of the samples were sputter coated with gold prior to SEM analysis. Fourier transform infrared (FT-IR) spectra were recorded by a Nicolet FT-IR 5700 spectrophotometer (Nicolet, Madison, USA) with 64 times of scans and the resolution of 4 cm^{-1}, and all the samples were dried before FT-IR experiment. The X-ray diffraction (XRD) was evaluated using diffractometer type D/max-Ra (Rigaku Co., Japan) with Cu target and Ka radiation (λ= 0.154 nm) at 40 kV and 50 mA at room temperature. The scanning rate was 0.5°/min and the scanning scope of 2θ was 1-10° and 5-60° in a fixed time mode.

2.4. Cytotoxicity assay

The prepared sponges were firstly cut into round disks (Diameter =6 mm),

transferred to the 96-well culture plates and sterilized by ethylene oxide gas, followed by incubating in DMEM medium at 37°C. They were then placed in the refrigerator for 24h, after the incubation period the so-called extracts were obtained and degermed by 0.22 μm filter prior to the following experiments.

The cytotoxicity of the CS/SA and CS-OREC/SA sponges to NHDFs was measured by MTT method [36]. A total of 1×10^4 NHDFs were seeded in 96-well microtiter plates and incubated in 200 μL Dulbecco modified eagle medium (DMEM) supplemented with 10% fetal bovine serum (FBS) and 1% penicillin/streptomycin. The culture medium were then removed and replaced with the extraction mentioned above and incubated for 24h, 72h and 120h, respectively. After that, the cells were washed gently with phosphate buffered saline (PBS) for three times, MTT (25 μL) was added into each well at 37°C for 4h, then DMSO (150 μL) was added to dissolve the MTT formazan purple crystals. Finally, the absorbance of the solution was measured at 490 nm by an enzyme linked immunosorbent assay (ELISA) Reader (MODEL550, Bio-Rad, USA).

2.5. Inhibition of bacterial activity

The method used for studying the bacterial inhibition activity of nanofibrous mats was reported previously [22, 37]. Gram-negative E. coli and Gram-positive Staphylococcus aureus (S. aureus) were selected as representative bacteria and cultivated in culture medium in an incubator. The antibacterial activities of CS/SA and CS-OREC/SA composite sponges were determined according to the disk diffusion method. The prepared specimens were sterilized under an ultraviolet

radiation lamp for 30 min and then cut in disks with the diameter of 20 mm, 50 uL diluted levitation bacterial with a concentration of 10^5-10^6 cfu/mL were inoculated into the agar culture medium uniformly. After that, the disks were placed on the surface of the agar medium at 37°C for 24h. The inhibition zones were measured with a tolerance of 1 mm. Each sample was repeated three times.

2.6. Evaluation of Hemostatic Effect

The male New Zealand White rabbits (wt 3-4 kg) of 4 months old were considered to characterize the hemostatic effect of CS/SA and CS-OREC/SA composite sponges. The experimental protocol was approved by the Ethics Committee for Animal Experimentation of the Fourth Military Medical University (TDLL-2014038, June 2014), which also met the Guide for the Care and Use of Laboratory Animals of the National Institutes of Health. The surgery was performed under anesthesia, and all efforts were made to minimize suffering. Experimental materials were sterilized by gamma ray (18 kGy).

For the ear artery injury and vein injury, the site of middle auricular artery and marginal auricular vein of rabbits were clipped and prepared after the anesthesia of intraperitoneal, respectively. Subsequently, it was bleed by transverse cut of the vessel using a scalpel blade. As the blood started flowing out from the wound, a piece of conventional sterile gauze was used to absorb the blood immediately. After 10 s of bleeding, the samples were placed at the wound and pressed lightly. The testing procedure was replicated five times for each material, and then calculated the mean hemostatic time and mean blood weight.

To establish liver injury model, rabbits were anesthetized and through abdomen section, liver was exposed. The wound was induced by an intersectional cut (0.5×0.5 cm) using a scalpel on the left medial lobe of liver. After 10 s of bleeding, the samples were put on the wounds and pressed lightly. The test procedure was replicated five times for each material, the bleeding times were recorded and the mean hemostatic times were calculated [38].

2.7. Statistics analysis

The values were expressed as means±standard deviation (SD). Whenever appropriate, two-tailed Student's t-test was used to discern the statistical difference between groups. A probability value (p) of less than 0.05 (*$p < 0.05$, **$p < 0.01$ or ***$p < 0.001$) was considered to be statistically significant.

3. Results and Dicussion

3.1. Characterization of CS-OREC/SA sponge

Figure 1 shows the FE-SEM images of both the surface and cross-section of the CS/SA and CS-OREC/SA sponges at two different magnifications. Dense pores with large size and uniform distribution were observed from the images of the surface of CS/SA (Figure 1 A). SA is an anionic polysaccharide, while the amino group of CS is positively charged. Their mixture produced a polyelectrolyte composite [39] and then porous sponges with three-dimensional structure were obtained through lyophilization. As shown in Figure 1C, the interconnected 3D porous structure and uniformity of the sponge was retained after the introduction of OREC, however, some other significant changes occurred with respect to pore size and morphology. The mean pore size increased from 100 μm for CS/SA to 135 μm for CS-OREC/SA. Interestingly, the cross-section morphologies of the CS/SA and CS-OREC/SA sponges are shown in Figure 1B and D. Sheet-like structure appeared in CS/SA together with condensed walls which were different from the surface morphology (Figure 1B). No big difference between the two sponges was observed except for the appearance of several fibers between adjacent pores after the intercalation of OREC (Figure 1D).

It is known that the microstructure including the pore size and its distribution has prominent influence on cell intrusion, proliferation and function in tissue engineering. The results indicated that the morphology difference is mainly caused by the CS-OREC intercalation and cross-linking process. The introduction of OREC might induce the fibers to be combined again to form sheets, leading to the fusion of some

smaller pores to generate larger ones.

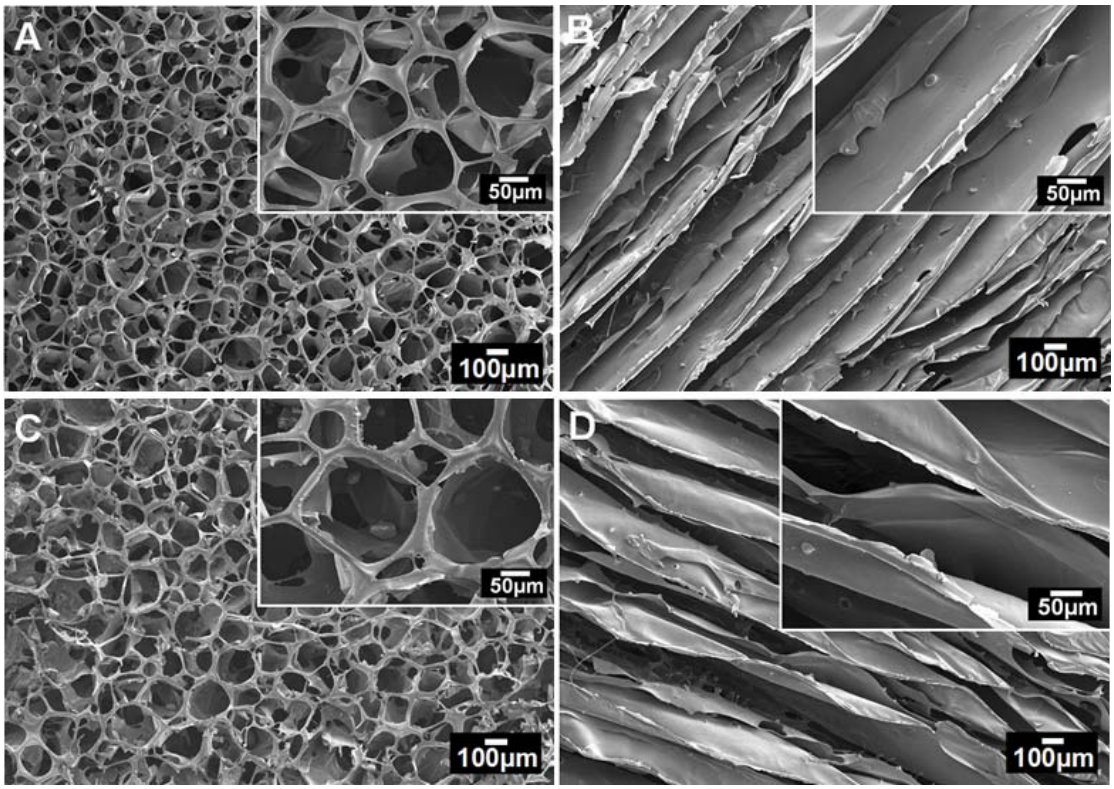

Fig. 1. FE-SEM images of surface (A) and cross-sectional (B) morphology of CS/SA sponge and surface (C) and cross-sectional (D) morphology of CS-OREC/SA sponge.

Figure 2 presents the FT-IR spectra and WAXRD patterns of bulk materials and resultant CS/SA and CS-OREC/SA composite samples. As shown in Figure 2A, the characteristic absorption peaks of CS were found at 3434 cm^{-1}, 1656 cm^{-1} and 1596 cm^{-1}, commonly ascribed to the N-H bonded to O-H vibration, amide I and amide II, respectively [22]. In the FT-IR spectrum of SA, a peak observed at 1616 cm^{-1} was attributed to the vibration of the C=O group, while the peak at 1419 cm^{-1} was related to symmetric and asymmetric stretching of the carboxylate group. The band at 1029 cm^{-1} was attributed to the stretching of the C-O-C bond [40]. OREC had the dominant peaks around 467 and 546 cm^{-1}, representing Si-O bending vibration. Besides, it had

characteristic adsorption peaks appearing at 2917 cm^{-1} and 2850 cm^{-1} which belong to -CH_2- and -CH_3 stretching vibrations [23, 32].

In the spectrum of the CS-OREC nanocomposites, the peak at 3642 cm^{-1} disappeared which indicated that the -OH of OREC had reacted with CS. Besides, the N-H and O-H vibrations at 3434 cm^{-1} in CS shifted to lower frequency (3411 cm^{-1}). This fact revealed that -NH_2 and -OH groups of CS formed hydrogen bonds with the -OH group of OREC. Another reason might be a strong hydrogen bonding interaction between CS molecules and inside CS molecules when constrained into the gallery of OREC layers [34]. As compared to the spectra of pure CS, the frequency of vibration bands at 1596 cm^{-1} which corresponded to the deformation vibration of the protonated amine group, were shifted towards lower frequency value of 1564 cm^{-1} in CS-OREC composites. This shift appeared as a result of the electrostatic interaction between amine groups and the negatively charged sites in the clay structure, and was consistent with result in previous report [31]. Besides, in the spectrum of CS/SA, the reaction of the carboxylic groups of alginate (ALG) with the amine groups of CS to form an anionic complex was already known [41]. Hence changes were expected in the absorption bands of these groups after complexation. As can be seen, the symmetrical stretching of COO- groups shifted to 1415 cm^{-1}, which revealed that the carboxylic groups of ALG had interacted with CS. As observed in Figure 2A-f, the peak at 3642 cm^{-1} disappeared which indicated that the -OH of OREC had reacted with CS or ALG. The dominant peaks of OREC at 489 cm^{-1} verified the successful deposition of OREC after solution intercalation.

The WAXRD patterns of bulk materials and resultant composite sponges are presented in Figure 2B, the crystal peak of CS near 20.24° (Fig. 2B-a) was clearly observed while the diffraction of OREC consisted of 7.33°, 8.65°, 11.56°, 20.1°, 27.50°, 29.65° and 35.58° (Fig. 2B-b). However, the crystal peak of OREC near 20.1°, 27.50°, 29.65° and 35.58° disappeared in CS-OREC composite, replacing by two stronger peak around 8.76° and 11.72°(Fig. 2B-c) which evidenced the successful deposition of OREC. Besides, new crystal peaks appeared at 18.78° and 23.56° verified the strong interaction of CS and OREC which resulted in the restriction of molecular movement of CS chains and destruction of crystallinity of CS. Moreover, SA appeared major crystal peaks around 13.74° and 21.88° (Fig. 2B-b), after the formation of CS/SA composites, the peaks appeared at 13.4° due to the incorporation of SA. Of note, new crystal peaks appeared at 18.54° and 23.3° which was also found in CS-OREC/SA. Interestingly, compared to the major peaks appeared at 20.1°, 27.50°, 29.65° and 35.58° of pure OREC, these of CS-OREC/SA gradually disappeared. The characteristic diffraction peaks of CS-OREC/SA appeared at 8.68°, 11.56°, 18.38° and 23.44° which confirmed the existence of OREC, CS and SA, but the diffraction heights at 8.68° and 11.90° were significantly reduced while the crystalline peak at 23.44° became wider. It was evident that the addition of OREC greatly changed the crystallinity of CS and SA. This fact confirmed the strong interaction between CS, SA and OREC as well, thus resulted in the restriction of molecular movement of CS and SA chains. This data suggested a lower crystallinity of CS and SA and improved miscibility of the prepared composite sponges.

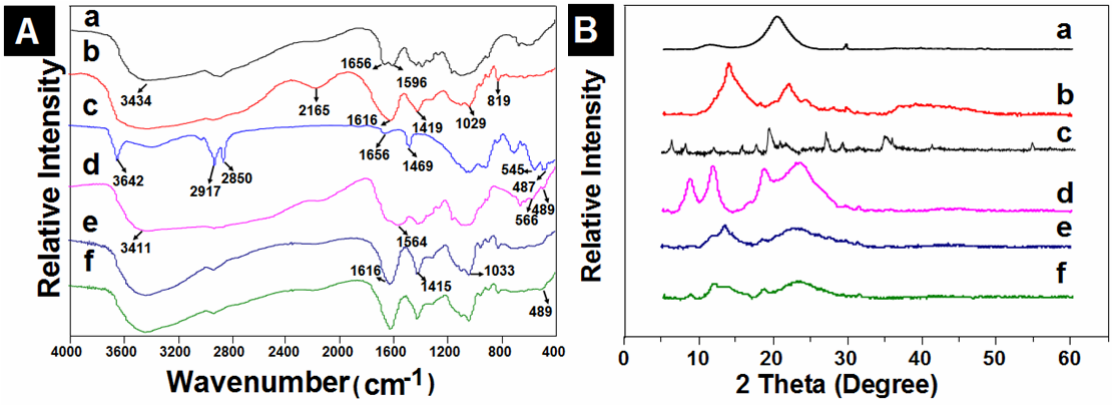

Fig. 2. FT-IR spectra (A) and WAXRD pattern (B) of (a) CS, (b) SA, (c) OREC, (d) CS-OREC, (e) CS/SA composite sponge and (f) CS-OREC/SA composite sponge.

Figure 3 shows the composition analysis results of the CS/SA and CS-OREC/SA composite samples by EDX analysis together with the SAXRD patterns and of OREC and CS-OREC/SA composite sponge. EDX spectra suggested the contents of Si and Al in CS-OREC/SA sponge (Figure 3B) were 4.84% and 5.91% while none of them were detected in CS/SA sponge (Figure 3A), respectively. It was well recognized that Al and Si were characteristic elements of OREC. As for the immobilized ability of OREC into various scaffolds, it has been reported that the contents of Si and Al are 1.97% and 1.44% in $(HTCC\text{-}OREC/SA)_{10.5}$ film-coated nanofibrous mats [27]. Herein, the detection of Si and Al was attributed to the successful intercalation of OREC into the CS and SA chains which was in accordance with the FE-SEM observation (Figure 1C). Hence, one can deduce from the above results that the composite sponges can act as excellent host for OREC due to the porous structure and uniform distribution of polymers. Moreover, SAXRD was employed to investigate the building of predesigned intercalated architecture in composite sponge (Figure 3C). OREC

exhibited 2θ=1.88° and the interlayer distance was 4.69 nm, calculated by the Braggs equation of nλ= 2d sinθ. In comparison with OREC, the peak of CS-OREC/SA intercalation composition shifted towards lower angle (2θ= 1.49°) and the interlayer distance was enlarged to 5.92 nm. The fact revealed that the CS and SA chains inserted into the intergallery of OREC.

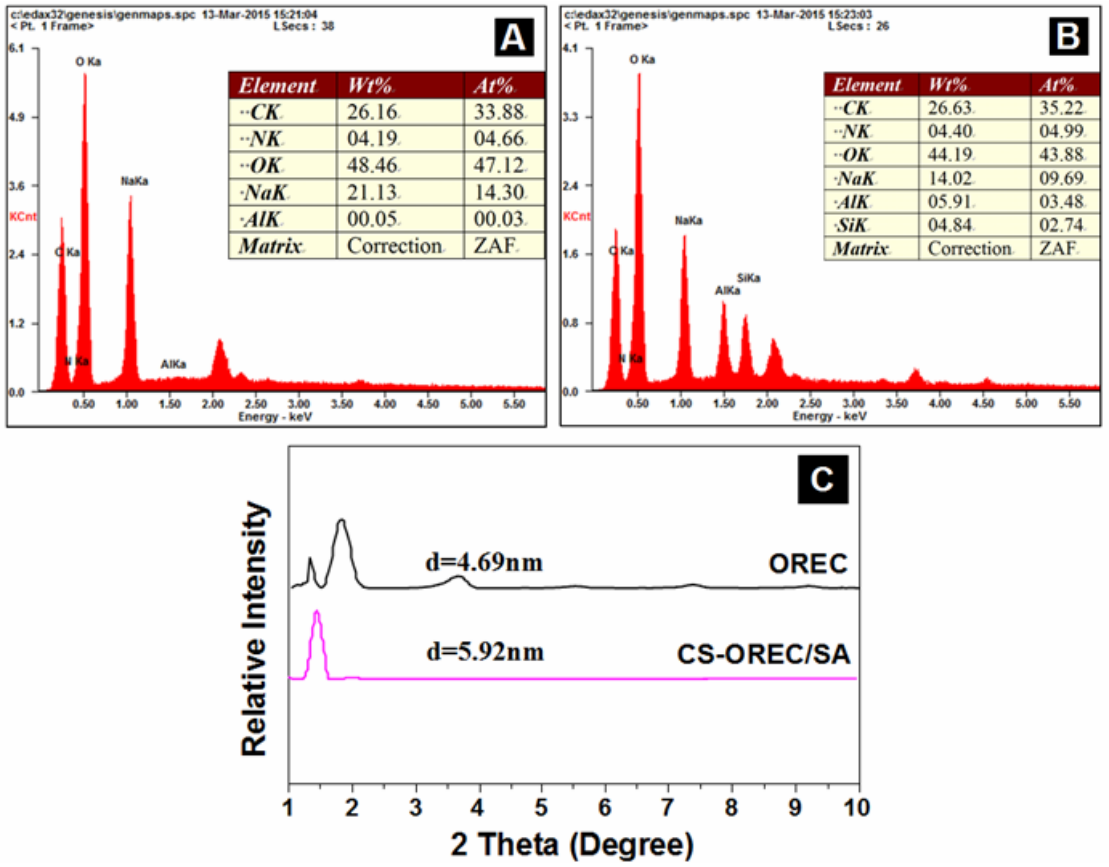

Fig. 3. EDX spectra of (A) CS/SA sponge and (B) CS-OREC/SA sponge; (C) SAXRD pattern of OREC and CS-OREC composite.

3.2. Cell viability test

To monitor cell adhesion and viability on different substrates, the number of cells was determined by using the colorimetric MTT assay. Figure 4 summarized the cell

viability on CS/SA and CS-OREC/SA along with 24h, 72h and 120h incubation. The cell culture plate (TCPS) was used as the control group, it showed that NHDFs cultured in both scaffolds exhibited a similar growth pattern of time-dependent increase of cell number during the culture period. In detail, the cell viability of CS/SA and CS-OREC/SA were 81.01±2.28% ($P<0.05$) and 87.59±4.39% on day 1, 98.66±6.92% and 109.50±3.38% on day 3, 115.55±3.29% and 124.20±3.92% on day 5. Besides, compared with the cell viability of NHDFs on CS/SA template, the addition of OREC into CS/SA during intercalation process led to higher cell viability. On days 3 after incubation, lower optical density was observed on TCPS than that on CS/SA and CS-OREC/SA, which was due to the 2D surface that was just suitable for the monolayer. When cells became confluent, contact inhibition resulted in the cease of mitosis. The data demonstrated the enhanced biocompatibility and supportiveness of CS-OREC/SA sponge for NHDFs proliferation.

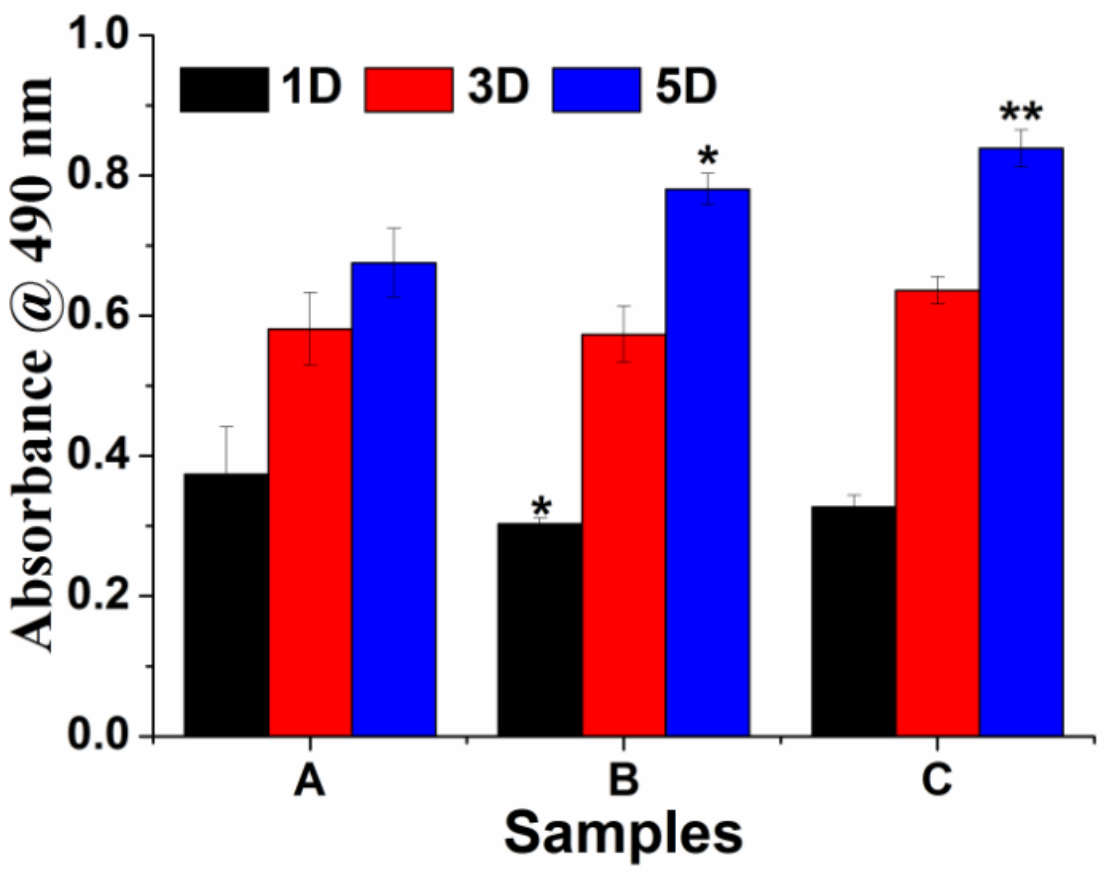

Fig. 4. The cell viability of L929 cells: (A) control group and cells cultured with (B) CS/SA sponge and (C) CS-OREC/SA sponge tested by MTT assay, significant difference: $^{*}p<0.05$, $^{**}p<0.01$, $^{***}p<0.001$.

3.3. Antibacterial Activity

The antibacterial features of CS/SA and CS-OREC/SA were evaluated against the Gram positive and negative bacteria, S. aureus and E. coli. Figure 5 shows the antibacterial activities of tested composite sponges by disc-agar diffusion tests. Apparently, the inhibitory property of both CS/SA and CS-OREC/SA sponges against the Gram-positive bacteria are better than that against Gram-negative bacteria which was consistent with the previous reports [42]. As observed in Figure 4A, the inhibition zones were around 5 mm against E. coli and 6.3 mm against S. aureus, respectively.

The antimicrobial activity might be attributed to the combined characteristics of CS and SA: on one hand, some researchers believed that CS killed bacteria through cell membrane damage duo to the electrostatic interactions between protonated amino groups of CS and phosphoryl groups of phospholipid components of cell membranes [43]. On the other hand, SA can easily form gel structure which will provide a beneficial physical barrier against bacteria based on the hydrogel properties [44]. Besides, as expected, the degree of bacterial inhibition was remarkably enhanced with the addition of OREC into the composite sponges. The inhibition diameters were around 7 mm against E. coli and 11 mm against S. aureus, respectively. In addition, both the CS/SA and CS-OREC/SA composite sponges exhibited partial dissolution when co-culturing with microorganism. It can be explained by the nutritive property of SA [45]. Taken together, the antibacterial activity of prepared composite sponge was improved with the introduction of OREC. The reason why the addition of OREC could significantly enhance the antibacterial efficiency could be concluded as follows: The positively charged OREC can absorb the negatively charged bacteria via electrostatic forces, and the bacteria can be immobilized on the surface of OREC [33]. Besides, OREC exhibits large surface area and adsorption capacity which could absorb bacteria and inhibit the proliferation of them [31]. More importantly, the bacterial adsorption and immobilization capacities of CS-OREC were synergistically improved because of its hydrophobicity and higher positive charge [23].

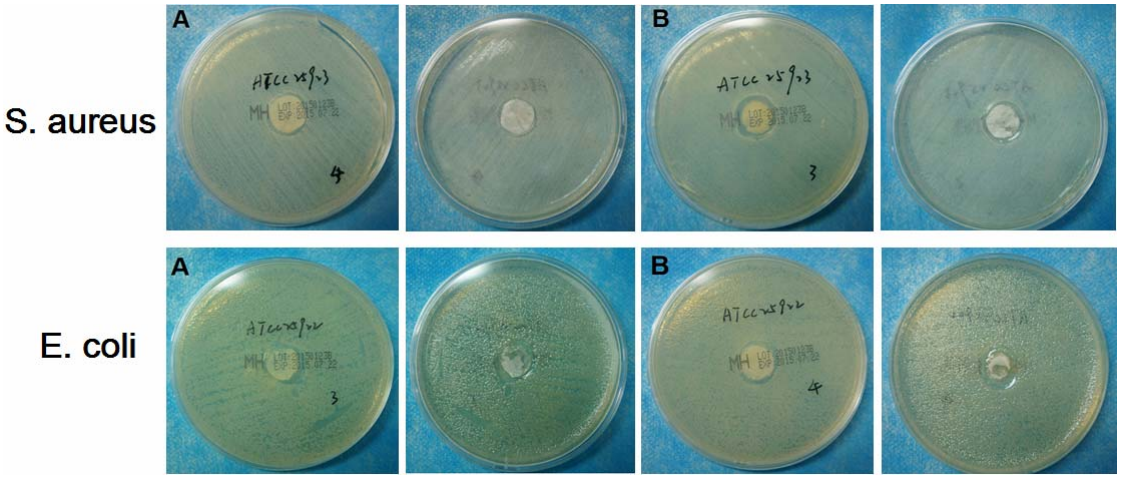

Fig. 5. Antibacterial activity of (A) CS/SA sponge and (B) CS-OREC/SA sponge.

3.4. Hemostatic Effects

The hemostatic efficacy of CS/SA and CS-OREC/SA sponge was evaluated by rabbit ear artery, ear vein and liver hemorrhage model. The mean bleeding time and mean blood weight of both composite sponges were summarized in Table 1. Figure 6 presented the conventional gauze (A-F) and CS-OREC/SA (A'-F') applied on marginal auricular vein and auricular artery of rabbit. The surface of the prepared sponge was soaked with a certain amount of blood, and it turned to be dark brown or black immediately and gradually to be a clot after contacting with blood. Finally, the bleeding was stopped in 97 seconds (vein) and 145 seconds (artery) in CS-OREC/SA treated group while bleeding was stopped in 137 seconds (vein) and 233 seconds (artery) in OREC-free sponge. But the changes were not statistically significant. Hence, for the OREC containing composite sponge, the arrest of bleeding took shorter time with less blood loss in comparison with the sponges without it.

The shape change of the CS-OREC/SA during arresting blood was greatly different

from CS/SA sponge (data not shown). Since the CS/SA sponge was partially water-soluble due to the –COONa group, the sponge could dissolve in the blood quickly and became transparent. The CS /SA gauze swelled and formed a coagulum at the bleeding site (data not shown). Although the coagulum gauze was beneficial to stop the vessel end bleeding, the gauze did not stand the shock of faster blood flow from the artery and was swept quickly away and could not arrest the later bleeding. Hence, the hemostatic efficacy of the CS/SA was relatively low in ear-artery bleeding. However, the OREC containing sponge still maintained the compact structure after covering on the ear wound. The reason might be that the mechanical property of the sponge was enhanced with the addition of OREC and the intercalation between CS and OREC and the agent went on performing the hemostatic function.

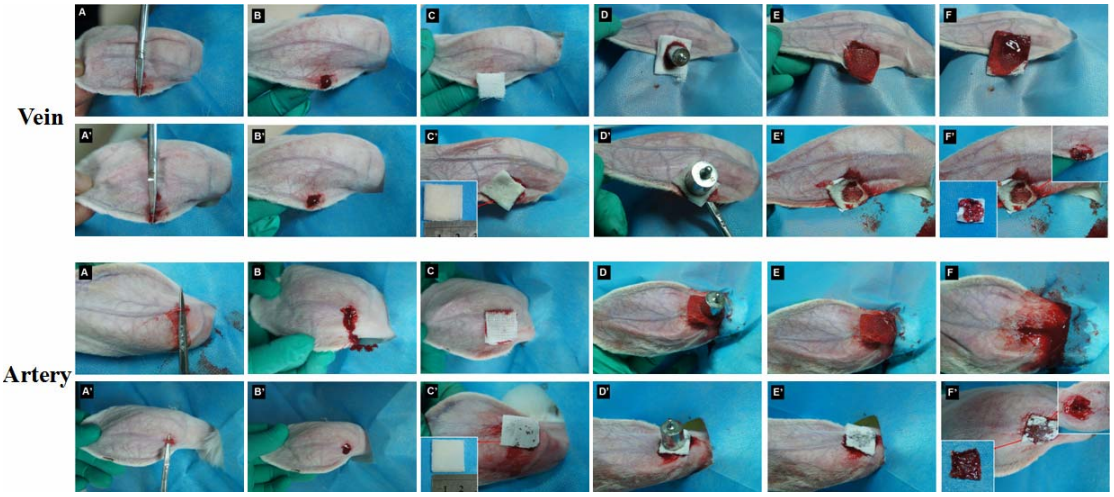

Fig. 6. The hemostatic effect of conventional medical gauze and prepared CS-OREC/SA sponge used to paste and press on the ear artery and auricular vein of rabbit.

Table 1. The mean hemostatic time (MHT) (s) and mean blood weight (MBW) (g) of (A) CS/SA and (B) CS-OREC/SA composite sponge in various rabbit injury models.

	MHT (s)			MBW (g)		
Sample	Ear artery	Ear vein	Liver	Ear artery	Ear vein	Liver
A	233±48	137±28	275±53	1.21±0.15	0.56±0.11	2.33±0.41
B	145±24	97±18	176±32	0.76±0.10	0.27±0.06	1.36±0.19

For the liver injury, consistent with these results of ear injury model, the styptic effect was stronger with the addition of OREC for the composite sponges (Figure 7). The CS-OREC/SA had higher hemostatic efficacy than CS/SA and gauze. It took longer time (275 s) with higher blood loss for CS/SA on arresting blood in comparison with CS-OREC/SA (176 s). As observed in the inset of Figure 7G, when the composite sponges were contacted with blood, they could stop bleeding quickly. The concentrated blood had higher viscosity and the blood flowing rate became low, finally the blood gradually clotted, its viscosity enhanced like well-known CMC which contributed to its hemostatic activity by adhering tightly to the wound surface to seal leaking.

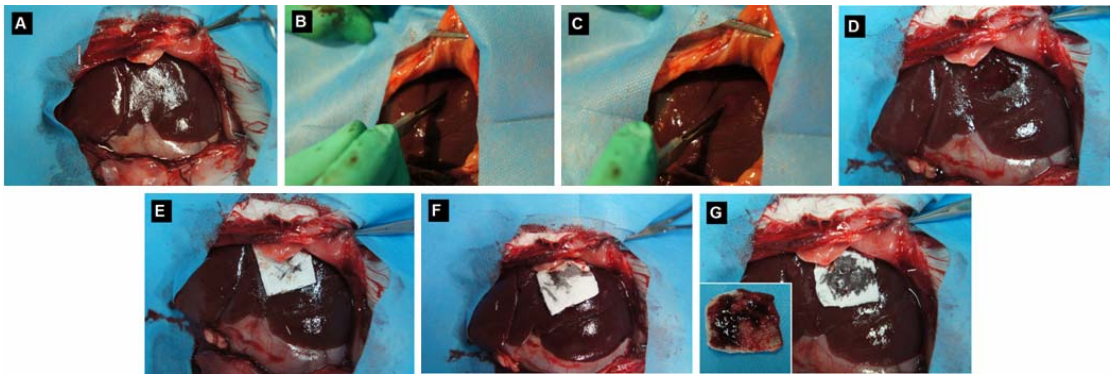

Fig. 7. The hemostatic effect of prepared CS-OREC/SA sponge applied in the rabbit liver trauma.

Based on the hemostatic effects demonstrated by the above models, the

CS-OREC/SA composite sponge exhibited higher hemostatic efficiency than CS-coated oxidized regenerated cellulose gauze reported by He *et al* [38]. It was reasonable to deduce that the styptic capacity of the composite sponges was remarkable improved with the introduction of OREC. The hemostatic behavior of the composite sponges may be mainly related to the structure and properties itself. Firstly, the CS is a proven and effective hemostat with hydrophilic property that could participate along with blood coagulation [46, 47]. In detail, the amino groups with positive charge of CS attracted the negative charge of muramic acid distributed on the surface of the red blood cells [11]. Therefore, it came out a strong adhesion effect leading to the aggregation of red blood cells so as to promote blood clotting and achieve hemostatic effect. Secondly, the water-soluble -COONa groups make the gauze rapidly gel when it contacts with the blood [38]. A lot of water in the blood was absorbed by the SA so that the density and viscosity of blood increased rapidly which made the blood flow slow down and achieved high blood clotting rate. What's more, the CS-OREC containing composite sponges had larger specific surface area than CS and swelling characteristics which contributed to the water-absorption. As a result, the composite sponges became a viscous gel covering on the surface of the wound.

4. Conclusion

In this paper, we reported the fabrication of porous CS-OREC/SA sponge by solution intercalation, cross-linking and freeze-drying techniques. The introduction of OREC had significant influence on the morphology of the sponge including pore size

and distribution. FT-IR, EDX and XRD results evidenced the interaction between CS and OREC and the successful assembling of OREC into CS/SA composites. Besides, the antibacterial activities of the CS-OREC/SA composite sponges which were helpful for inhibiting the inflammation of the wound were greatly improved compared to CS/SA. Moreover, the CS/SA and CS-OREC/SA composite sponge was evaluated for possible application as a hemostatic agent in clinical treatments. The hemostatic test of the rabbit liver, ear-artery and ear-vein injury demonstrated that the introduction of the OREC into the crosslinked sponge improved the styptic capacity. The prepared composite sponge was more suitable as the hemostatic material applied in the rabbit liver trauma in comparison with the ear-artery trauma. These results suggested that the OREC-contained composite sponges could be applied as a new kind of effective hemostat, which showed great potential in clinical application.

Acknowledgements

This project was funded by National High Technology Research and Development Program of China (863 Program) (Grant No: SS2015AA020313), National Natural Science Foundation of China (Grant Nos: 81272134, 81171804, 81071570, 81401597) and Science and Technology Innovation Development Foundation of Tangdu hospital (Grant No: 2013CXTS016).

References

1. D. S. Kauvar, R. Lefering and C. E. Wade, *Journal of Trauma and Acute Care Surgery*, 2006, **60**, S3-S11.

2. J. G. McManus, B. J. Eastridge, C. E. Wade and J. B. Holcomb, *Journal of Trauma and Acute Care Surgery*, 2007, **62**, S14.

3. A. Sauaia, F. A. Moore, E. E. Moore, K. S. Moser, R. Brennan, R. A. Read and P. T. Pons, *Journal of Trauma and Acute Care Surgery*, 1995, **38**, 185-193.

4. B. S. Kheirabadi, A. Field-Ridley, R. Pearson, M. MacPhee, W. Drohan and D. Tuthill, *Journal of Surgical Research*, 2002, **106**, 99-107.

5. P. Rhee, C. Brown, M. Martin, A. Salim, D. Plurad, D. Green, L. Chambers, D. Demetriades, G. Velmahos and H. Alam, *Journal of Trauma and Acute Care Surgery*, 2008, **64**, 1093-1099.

6. I. Wedmore, J. G. McManus, A. E. Pusateri and J. B. Holcomb, *Journal of Trauma and Acute Care Surgery*, 2006, **60**, 655-658.

7. N. Ahuja, T. A. Ostomel, P. Rhee, G. D. Stucky, R. Conran, Z. Chen, G. A. Al-Mubarak, G. Velmahos and H. B. Alam, *Journal of Trauma and Acute Care Surgery*, 2006, **61**, 1312-1320.

8. K. R. Ward, M. H. Tiba, W. H. Holbert, C. R. Blocher, G. T. Draucker, E. K. Proffitt, G. L. Bowlin, R. R. Ivatury and R. F. Diegelmann, *Journal of Trauma and Acute Care Surgery*, 2007, **63**, 276-284.

9. C. K. Murray, S. A. Roop, D. R. Hospenthal, D. P. Dooley, K. Wenner, J. Hammock, N. Taufen and E. Gourdine, *Bacteriology of war wounds at the time of injury*,

DTIC Document, 2006.

10. M. Ip, S. L. Lui, V. K. Poon, I. Lung and A. Burd, *Journal of Medical Microbiology*, 2006, **55**, 59-63.

11. H. Zhong, W. Ye, X. Li, X. Wang and R. Sun, *Current Nanoscience*, 2013, **9**, 742-746.

12. S. Ong, J. Wu, S. M. Moochhala, M. Tan and J. Lu, *Biomaterials*, 2008, **29**, 4323-4332.

13. J. Fong and F. Wood, *international Journal of Nanomedicine*, 2006, **1**, 441.

14. V. K. Poon and A. Burd, *Burns*, 2004, **30**, 140-147.

15. J. G. Clay, D. Zierold, K. Grayson and F. D. Battistella, *Journal of Surgical Research*, 2009, **155**, 89-93.

16. A. E. Pusateri, J. B. Holcomb, B. S. Kheirabadi, H. B. Alam, C. E. Wade and K. L. Ryan, *Journal of Trauma and Acute Care Surgery*, 2006, **60**, 674-682.

17. N. Bhattarai, D. Edmondson, O. Veiseh, F. A. Matsen and M. Zhang, *Biomaterials*, 2005, **26**, 6176-6184.

18. X. Yang, X. Chen and H. Wang, *Biomacromolecules*, 2009, **10**, 2772-2778.

19. M. C. Bonferoni, G. Sandri, S. Rossi, F. Ferrari and C. Caramella, *Expert Opinion on Drug Delivery*, 2009, **6**, 923-939.

20. L. Ma, C. Gao, Z. Mao, J. Zhou, J. Shen, X. Hu and C. Han, *Biomaterials*, 2003, **24**, 4833-4841.

21. F. Mi, S. Shyu, Y. Wu, S. Lee, J. Shyong and R. Huang, *Biomaterials*, 2001, **22**, 165-173.

22. H. Deng, P. Lin, S. Xin, R. Huang, W. Li, Y. Du, X. Zhou and J. Yang, *Carbohydrate polymers*, 2012, **89**, 307-313.

23. H. Deng, X. Wang, P. Liu, B. Ding, Y. Du, G. Li, X. Hu and J. Yang, *Carbohydrate polymers*, 2011, **83**, 239-245.

24. T. Hashimoto, Y. Suzuki, M. Tanihara, Y. Kakimaru and K. Suzuki, *Biomaterials*, 2004, **25**, 1407-1414.

25. K. Murakami, H. Aoki, S. Nakamura, S.-i. Nakamura, M. Takikawa, M. Hanzawa, S. Kishimoto, H. Hattori, Y. Tanaka and T. Kiyosawa, *Biomaterials*, 2010, **31**, 83-90.

26. Y. Chung, Y. Su, C. Chen, G. Jia, H. Wang, J. Wu and J. Lin, *Acta Pharmacologica Sinica*, 2004, **25**, 932-936.

27. R. Huang, Y. Li, X. Zhou, Q. Zhang, H. Jin, J. Zhao, S. Pan and H. Deng, *Carbohydrate polymers*, 2012, **90**, 957-966.

28. X. Wang, B. Liu, J. Ren, C. Liu, X. Wang, J. Wu and R. Sun, *Composites Science and Technology*, 2010, **70**, 1161-1167.

29. European Food Safety Authority (EFSA), *EFSA Journal*, 2011, **9**, 2007-2030.

30. Y. Feng, J. Gong, G. Zeng, Q. Niu, H. Zhang, C. Niu, J. Deng and M. Yan, *Chemical Engineering Journal*, 2010, **162**, 487-494.

31. X. Wang, B. Liu, X. Wang and R. Sun, *Current Nanoscience*, 2011, **7**, 183-190.

32. H. Deng, X. Li, B. Ding, Y. Du, G. Li, J. Yang and X. Hu, *Carbohydrate polymers*, 2011, **83**, 973-978.

33. X. Wang, Y. Du, J. Luo, J. Yang, W. Wang and J. F. Kennedy, *Carbohydrate*

polymers, 2009, **77**, 449-456.

34. X. Wang, Y. Du, J. Yang, X. Wang, X. Shi and Y. Hu, *Polymer*, 2006, **47**, 6738-6744.

35. R. Huang, X. Zhou, X. Liu, Q. Zhang, H. g. Jin, X. Shi, W. Luo and H. Deng, *Journal of biomedical nanotechnology*, 2014, **10**, 485-499.

36. R. Huang, W. Li, X. Lv, Z. Lei, Y. Bian, H. Deng, H. Wang, J. Li and X. Li, *Biomaterials*, 2015, **53**, 58-75.

37. W. Huang, X. Li, Y. Xue, R. Huang, H. Deng and Z. Ma, *International journal of biological macromolecules*, 2013, **53**, 26-31.

38. J. He, Y. Wu, F. Wang, W. Cheng, Y. Huang and B. Fu, *Fibers and Polymers*, 2014, **15**, 504-509.

39. J. Jia, Z. Wang, W. Lu, L. Yang, Q. Wu, W. Qin, Q. Hu and B. Z. Tang, *Journal of Materials Chemistry B*, 2014, **2**, 8406-8411.

40. A. Abruzzo, F. Bigucci, T. Cerchiara, B. Saladini, M. C. Gallucci, F. Cruciani, B. Vitali and B. Luppi, *Carbohydr Polym*, 2013, **91**, 651-658.

41. D. Liu, X. Yuan and D. Bhattacharyya, *Journal of Materials Science*, 2012, **47**, 3159-3165.

42. W. Li, X. Li, Y. Chen, X. Li, H. Deng, T. Wang, R. Huang and G. Fan, *Carbohydrate polymers*, 2013, **92**, 2232-2238.

43. H. K. No, N. Y. Park, S. H. Lee and S. P. Meyers, *International journal of food microbiology*, 2002, **74**, 65-72.

44. S. A. Covarrubias, L. E. de-Bashan, M. Moreno and Y. Bashan, *Applied*

microbiology and biotechnology, 2012, **93**, 2669-2680.

45. S. H. Yu, F. L. Mi, Y. B. Wu, C. K. Peng, S. S. Shyu and R. N. Huang, *Journal of applied polymer science*, 2005, **98**, 538-549.

46. X. Huang, Y. Sun, J. Nie, W. Lu, L. Yang, Z. Zhang, H. Yin, Z. Wang and Q. Hu, *International journal of biological macromolecules*, 2015, **75**, 322-329.

47. X. Huang, J. Jia, Z. Wang and Q. Hu, *Chin J Polym Sci*, 2015, **33**, 284-290.